JOURNAL OF SPACECRAFT AND ROCKETS
Vol. 47, No. 6, November–December 2010

Magnus and Spin-Damping Measurements of a Spinning Projectile Using Design of Experiments

Se-Yoon Oh,* Sung-Cheol Kim,† Do-Kwan Lee,† Sangho Kim,‡ and Seung-Ki Ahn‡
Agency for Defense Development, Daejeon 305-600, Republic of Korea

DOI: 10.2514/1.50188

The purpose of this research is to efficiently characterize the dynamic Magnus effect and spin-damping data of a spinning projectile or missile over the required experimental region using statistically designed experiments for wind-tunnel tests. In the present work, the wind-tunnel tests for the Magnus effect and spin-damping measurements were conducted on a 155-mm spin-stabilized projectile model. The tests used techniques involving the design of the experiments and response surface modeling. The Magnus effect and spin-damping data were investigated for various Mach numbers and angle-of-attack combinations. The validity of the wind-tunnel measurement techniques was evaluated by comparing them with the previous test results on the same configuration. The experimental results show that regression models were found to successfully estimate the Magnus effect and spin-damping needed to investigate aerodynamic characteristics of a spinning projectile over the required experimental design space.

Nomenclature

C_l = rolling moment coefficient, l/qSd
C_{l_p} = spin or roll-damping coefficient
C_n = yawing moment coefficient relative to model nose tip, n/qSd
C_{n_p} = Magnus moment derivative
C_Y = side-force coefficient, Y/qS
C_{Y_p} = Magnus side-force derivative
d = reference body diameter or maximum diameter, ft
I_x = roll moment of inertia of the spinning mass, slug·ft^2
L = model overall length, ft
l = rolling moment; body axis system, in · lb
M = Mach number
n = yawing moment; body axis system, in · lb
p = model spin rate or roll rate, rad/s
q = freestream dynamic pressure, psf
S = missile reference area, $\pi d^2/4$
t = time, s
U_r = 95% confidence uncertainty
V = freestream velocity, ft/s
Y = side force; body axis system, lb
α = angle of attack, deg
ψ = angle of yaw, deg

I. Introduction

THE statistical design of experiments (DOE) approach to wind-tunnel testing of a spin-stabilized projectile is being investigated. An exploratory study was completed using response surface methodology (RSM) in an effort to efficiently characterize projectile aerodynamics as a function of attitude and Mach number inputs. Dynamic stability derivatives such as the Magnus dynamic effects and spin-damping coefficients are important in determining targeting accuracy of spinning missiles or projectiles. It is generally considered that an indoor spark photography range test and a telemetry free-flight test will undoubtedly be the most accurate approaches in obtaining the full set of dynamic spin-damping and Magnus effects [1–3]. During the design phase, an engineering code or wind-tunnel testing is usually used to develop candidate designs that are then fired in the spark range to confirm the aerodynamics; however, these free-flight measurements are both expensive and time consuming. Therefore, the use of computational fluid dynamics (CFD) calculations and wind-tunnel experiments can be effective means to assist in the new low-cost development of advanced projectile systems. In the projectile field, the ability to predict the full set of aerodynamic coefficients for stability and performance assessment for various projectiles using CFD has been extensively used. DeSpirito and Heavey [2], Sahu [3,4], Weinacht [5,6], DeSpirito et al. [7,8], and Stahl et al. [9,10] have made significant contributions in this regard. Wind-tunnel testing can be an alternative method for Magnus effect and spin damping due to the fullness of the data set, although its results should be corrected and validated by a free-flight test. Before the present work, several experimental studies were conducted to optimize the design configuration and to investigate aerodynamic coefficient characterization such as the static aerodynamic coefficients, model base drag measurements, and the effects of base configurations (the boat-tail angles, the bore rider angles, and wheelbases) on the static and Magnus coefficients. The discussion herein is mainly focused on effective statistical methodologies that are applied to the wind-tunnel measurements by comparing prior wind-tunnel test results.

The dynamic loads, such as the Magnus effect and spin damping, are usually small relative to the static loads, and they are hard to measure with reasonable accuracy because they must be measured with the model in motion. These parameters have often been estimated rather than measured because of a limited budget for the testing and the higher priority to acquire static stability and drag data during the wind-tunnel entries [11,12]. Insufficient estimation of these roll-based parameters is likely to cause a substantial change in vehicle trajectory and flight characteristics; hence, a more reliable approach to the wind-tunnel tests is required to reduce the test resources (time and cost) and improve the test accuracy. Given the significance of the dynamic stability derivatives of spinning missiles or projectiles, the accuracy and quality of the experimental data should be assured so that the quantitative estimates of test uncertainties can be provided. Although various works [13–18] have focused on the measurements of dynamic stability derivatives for models in roll motion, statistical DOE-based testing techniques for a spinning model in wind-tunnel testing are rare, because most wind-tunnel tests are based on the traditional experiments focused on conventional one-factor-at-a-time [19,20] methods, a time-consuming process that makes wind-tunnel testing very expensive.

Presented as Paper 2009-5844 at the AIAA Atmospheric Flight Mechanics Conference, Chicago, IL, 10–13 August 2009; received 5 April 2010; revision received 13 September 2010; accepted for publication 14 September 2010.

*Senior Researcher, Aerodynamics Branch, Wind Tunnel Test Branch. Senior Member AIAA.
†Senior Researcher, Aerodynamics Branch, Wind Tunnel Test Branch.
‡Principal Researcher, Aerodynamics Branch, Wind Tunnel Test Branch.

To establish a reliable aerodynamic response model and a dynamic testing process for a spinning model, we first need to determine the tunnel control variables as design variables on the dynamic Magnus effect and spin-damping characteristics. In the present work, we considered two factors as design variables for the purpose of developing mathematical response models for the Magnus effect and spin damping of a scaled model of the spinning projectile. The two factors are the test Mach number M and the angle of attack (AOA) of the model α based on the body axis. We chose the DOE-based RSM (DOE/RSM) to investigate the effects of the design variables. The DOE/RSM technique has been widely used in recent wind-tunnel experiments, and a number of studies that use the DOE/RSM technique for wind-tunnel tests have been published. Favaregh and Landman [17], Omran et al. [18], DeLoach [21–23,25,27], DeLoach and Cler [24], and Landman et al. [26,28,29] have made significant contributions in this regard. The first part of this paper mostly investigates the nature of the Magnus effect and presents the dynamic test rig. The second part focuses on the DOE/RSM technique as a means of testing an approach for the spinning model. Finally, the experimental results are presented for the Magnus effect and spin-damping derivatives based on the DOE/RSM technique.

II. Experimental Details

The purpose of the Magnus test rig [2–8,11–13,15,16] is to measure the lateral force generated on a model rotating at high speed by the Magnus effects due to the unsymmetrical boundary layer of a rotating model during pitching. As shown in Fig. 1, the present Magnus model has characteristics that are very common in spinning projectiles: namely, the forebody and the boat-tail afterbody with a rotating band. The rotating band was fabricated with grooves to simulate an engraved band in flight, as can be seen in Fig. 2.

The Magnus effects reflect the change in the side force and yawing moment with respect to the decay in spin rate. The net side force and yawing moment generated by the spinning model are proportional to the spin rate and therefore change as the model spin rate decreases due to damping during a run. The Magnus coefficients are defined by the first derivatives of the side-force and yawing moment coefficients with respect to the nondimensional spin parameter. The Magnus force-and-moment derivatives are defined as follows:

$$C_{Y_p} = \partial C_Y / \partial (pd/2V) \tag{1}$$

$$C_{n_p} = \partial C_n / \partial (pd/2V) \tag{2}$$

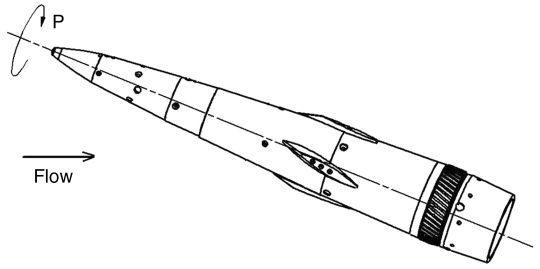

Fig. 1 Model configuration of the 155-mm spinning projectile.

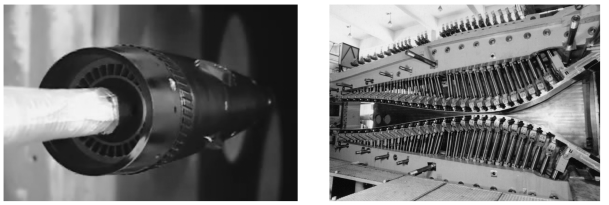

Fig. 2 Magnus/spin-damping test setup and flexible nozzle in the ADD-TSWT.

where $pd/2V$ is the nondimensional spin parameter or reduced frequency parameter. These Magnus dynamic derivatives for the spinning model are obtained by fitting linear equations to side-force coefficient and yawing moment coefficient data with respect to the nondimensional spin parameter, which is proportional to the model spin rate.

When a model is subjected to a rotational movement, the aerodynamic loads on the spinning model generate a rolling moment, tending to slow down the rotation. The spin-damping coefficient is the first derivative of the rolling moment coefficient, and it is defined in the following equation as the rate change of the rolling moment with respect to the nondimensional spin parameter:

$$C_{l_p} = \partial C_l / \partial (pd/2V) \tag{3}$$

The spin-damping moment is usually a derived parameter rather than directly measured and determined from the measured model spin rate decay of the model during the tunnel run time [11–13,15]. The spin-damping moment is determined from the measured spin rate decay of the model during a run. The model roll rate decay represents the total damping, including both the aerodynamic damping of the spinning model and the friction damping of the test mechanism. This friction damping should be subtracted from the total damping to obtain the desired aerodynamic damping. The spin-damping coefficient can be obtained from a simplified equation of motion with a free-spin technique for wind-tunnel experiments [13]. If I_x and two different (p, t) values are known from a measured spin-decay run, then the parameter C_{l_p} can be calculated. The spin-damping coefficient is defined as follows:

$$C_{l_p} = \frac{I_x}{(t_2 - t_1)} \ell_n \left(\frac{p_2}{p_1}\right) \left(\frac{2V}{qSd^2}\right) \tag{4}$$

where the assumptions that the system is exponentially damped and the roll parameters are constant over the given time intervals to obtain the spin-damping data are adopted.

The dynamic test rig in this work is a free-spin-decay system capable of rotating the model up to 20,000 rpm. Two ball bearings are used with the static force-and-moment balance to investigate the Magnus dynamic effects. An air-driven turbine is located near the base of the model, with the air exhausting out of the model base into the wake region, as can be seen in Fig. 3. An air-operated piston is located at the front of the roll-sleeve adapter and is used to lock the model before a free-spin-decay measurement is started. The driving torque of the Magnus rig is 30 in · lb at the operating air pressure of 500 psia. The rotating speed is measured by two optical photo sensors and a revolutions-per-minute (RPM) pickup plate. Usually, these optical sensors need a smaller space for installation, and they

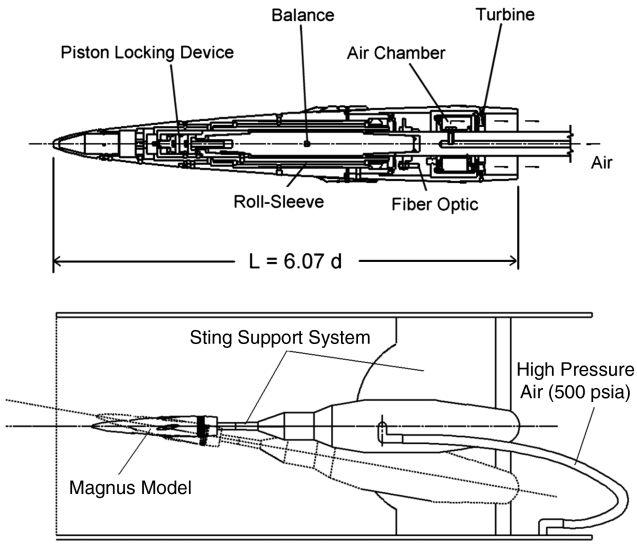

Fig. 3 Magnus/spin-damping test mechanism in the ADD-TSWT.

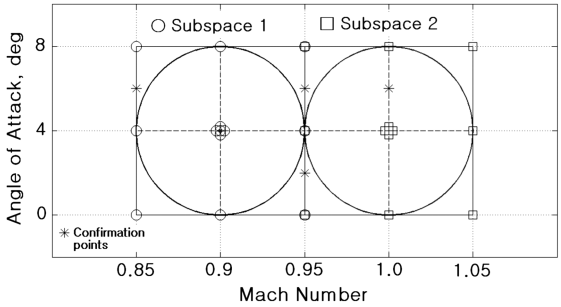

Fig. 4 FCCD for the DOE/RSM experiments (natural values).

measure a rotational speed without mechanical contact. One photo sensor reads the pattern signal from the RPM pickup plate and another sensor measures an azimuth angle of a rotating model. The bearing friction damping was determined before the test and subtracted from the total damping to obtain the desired spin-damping coefficients. The model moment of inertia was also measured and applied to the spin-damping data reduction. The axial force coefficient was corrected for the model base pressure and cavity pressure from the pressure tube reading to yield the forebody axial force coefficient.

Experiments were carried out in the high-speed wind tunnel to obtain the Magnus effect and spin-damping data for various Mach numbers and AOA combinations. The trisonic wind tunnel at the Agency for Defense Development (ADD-TSWT) is a blowdown tunnel with a transonic test section with porous walls of 6% porosity. The test section has an area of 4×4 ft, and the Mach number range is 0.4 to 4.0 (Fig. 2). The run time is from 15 to 45 s (depending on the Mach number and the range of model attitude). Aerodynamic forces and moments were measured with an internal six-component strain gauge balance at the sampling frequency of 50 Hz. A KB-41 internal six-component strain gauge balance (gauged and calibrated by Micro Craft Technology, San Diego, California) was used. The load ranges of the balance are as follows: side force up to 1200 lb and yawing moment up to 1800 in · lb. The overall accuracy of the balance is within $\pm 0.1\%$ of the full scale. The test Mach numbers ranged from 0.7 to 2.0, and the AOAs ranged from -4 to $+10$ deg. The nominal Reynolds number was 7.6 million per foot for most cases. All the tests were conducted at 12,000 rpm, corresponding to the nondimensional spin parameter ($pd/2V$) of 0.157, and the spinning model was dynamically balanced (± 0.03 in · gm). The present work concerns the way the dynamic Magnus effect and spin-damping characteristics due to model roll motion are investigated using DOE/RSM techniques for the model of a scaled-down spin-stabilized projectile with four canted bore riders on the forebody section at transonic/supersonic speeds. Figure 3 illustrates the 76% scale 155-mm spinning model mounted with a rear sting support in the ADD-TSWT facility.

As the main purpose of this work is to estimate the Magnus effect and spin-damping coefficients of a spinning projectile, the range of independent variables was partitioned into subranges that are small enough to fit aerodynamic data with a simple low-order regression function. We simply divided two different Mach number ranges (that is, transonic and supersonic Mach ranges). The central composite design [17–20,26–30] is the most popular class of designs used for fitting a second-order regression model. In the present study, a DOE with a face-centered composite design (FCCD) [19,20,29,30] is applied to the RSM to determine how the design parameters affect the Magnus effect and spin-damping characteristics. The experimental design variables in this work are the Mach number and the AOA. We can get a side-force coefficient slope and a yawing moment coefficient slope with respect to the reduced spin parameter from a free-spin-decay test for each FCCD experiment point. We assumed that the Magnus force and moment are almost a linear function of this spin parameter. Thus, the Magnus effects are calculated from the linear regression [11–14]. The spin-damping coefficient can also be calculated using this spin-decay data. Two subspaces [27] were chosen to examine the effect of the Mach number and AOA, because the highly nonlinear effect is not expected to be significant, as the Magnus effects and spin damping are usually linear at low AOAs. The FCCD experiments (Fig. 4) on M and α combinations (with a α range from 0 to $+8$ deg corresponding to ± 1 in the coded value) were conducted for the two subspaces, as can be seen in Fig. 4. The two design factors with three levels are summarized in Table 1. In the FCCD test matrix, the factor of interest is denoted in the coded level (linear transformed level), given in Table 1. We also tested extra $M - \alpha$ combinations as confirmation experiments.

The least-squares regression technique is usually applied to fit the RSM. This regression [19–22] is quite different from the ordinary regression, because the regression in the DOE/RSM is a predefined-designed regression for a DOE approach. This DOE/RSM-based regression provides us with mathematical response models of longitudinal static stability derivatives as a function of all the design factors in Table 1. The regression models used in the present study are of a second-order form, as given in the following equation:

$$y = \beta_0 + \sum_{i=1}^{k} \beta_i x_i + \sum_{i=1}^{k} \beta_{ii} x_i^2 + \sum_{i=1}^{k-1} \sum_{j=2}^{k} \beta_{ij} x_i x_j + \varepsilon \qquad (5)$$

for observations, where

$$x_i = \frac{\xi_i - [\max(\xi_i) + \min(\xi_i)]/2}{[\max(\xi_i) - \min(\xi_i)]/2}$$

where each β is a model coefficient to be determined empirically; each x is a regressor; y is a response variable, such as the pitching moment coefficient; and ε is a normally and independently distributed random error or residual assumed to have a zero mean value and a constant variance. The variable x_i in Eq. (5) transforms the natural or actual variable ξ_i so that the value falls between -1 and $+1$, as in Table 1.

III. Results and Discussion

A. Experimental Data and Analysis

The parameters C_{Y_p}, C_{n_p}, and C_{l_p} of a spinning model were obtained by varying M and α, as specified in the FCCD matrix of Fig. 4. These Magnus dynamic data for the spinning model were obtained by using a least-squares fit for each spin-decay run. The parameters C_{Y_p} and C_{n_p}, with respect to the spin parameter, were then calculated. The test results are summarized in Table 2. The uncertainty estimates [31,32] of various measurements of the present work were carried out in accordance with the AIAA standard S-017A-1999 [31]. The uncertainties in the aerodynamic static force-and-moment coefficients for the 155-mm projectile model are

Table 1 Factor levels for FCCD experiments

			Natural level (ξ_i)			Coded level (x_i)		
	Name	Factor	Low	Center	High	Low	Center	High
Subspace 1	Mach	M	0.85	0.9	0.95	−1	0	+1
	AOA, deg	α	0	+4	+8	−1	0	+1
Subspace 2	Mach	M	0.95	1.0	1.05	−1	0	+1
	AOA, deg	α	0	+4	+8	−1	0	+1

Table 2 FCCD matrix for experiments and measured results (subspace 1)

STD no.	Run no.	M	α, deg	C_{Y_p}	C_{n_p}	C_{l_p}
8	1	0.90	8	−0.14052	0.58366	−0.02803
2	2	0.95	0	0.01459	−0.06754	−0.02573
9	3	0.90	4	−0.06353	0.26953	−0.02753
13	4	0.90	4	−0.07290	0.26729	−0.02664
4	5	0.95	8	−0.14073	0.66317	−0.02637
11	6	0.90	4	−0.04290	0.21518	−0.02741
7	7	0.90	0	0.01549	−0.06782	−0.02689
12	8	0.90	4	−0.06297	0.24926	−0.02722
3	9	0.85	8	−0.11279	0.51136	−0.02807
5	10	0.85	4	−0.02380	0.15788	−0.02853
1	11	0.85	0	0.00446	−0.02846	−0.02779
10	12	0.90	4	−0.05680	0.26197	−0.02765
6	13	0.95	4	−0.06422	0.28272	−0.0262

Table 3 Estimated uncertainties ($M = 0.7$ and $\alpha = 5.96$ deg)

Response	Uncertainties (U_r)	Name
C_A	±0.0035	Axial force
C_Y	±0.0194	Side force
C_N	±0.0203	Normal force
C_l	±0.0063	Rolling moment
C_m	±0.0337	Pitching moment
C_n	±0.0455	Yawing moment
M	±0.0012	Mach number
α	±0.0320 deg	AOA

summarized in Table 3. The aerodynamic coefficients were based on the reference area S, and the moment coefficients were referenced to the nose tip of the model. The order of all the test runs was randomized to average out the influence of unknown variables over time. The tests were repeated five times about the center point ($M = 0.9$ and $\alpha = 4$ deg for subspace 1) of the FCCD matrix. Repeated runs of the same test achieved repeatability values of $C_{Y_p} = \pm 0.01107$, $C_{n_p} = \pm 0.02237$, and $C_{l_p} = \pm 0.00040$.

The Minitab [33] and the Design-Expert [34] software packages were used for data processing of the FCCD matrix generation, regression analysis, and analysis of variance (ANOVA). Table 4 gives regression analysis results of C_{Y_p} in coded units. The coefficients represent the mean change in response C_{Y_p} for one unit of change of the corresponding factor, holding other factors constant.

Table 4 Estimated regression coefficients for C_{Y_p} (subspace 1)[a]

Term	Coefficient	Standard errors	t for H_0 coefficient = 0	P value	Significance ($P < 0.05$)
Constant	−0.058177	0.005083	−11.446	0.000	Significant
M	−0.009705	0.004997	−1.942	0.093	Not significant
α	−0.071430	0.004997	−14.294	0.000	Significant
M^2	0.010059	0.007365	1.366	0.214	Not significant
α^2	−0.008446	0.007365	−1.147	0.289	Not significant
$M\alpha$	−0.009518	0.006120	−1.555	0.164	Not significant

[a]$R^2 = 96.82\%$, and $R^2(\text{adj}) = 94.54\%$.

Table 5 Estimated regression coefficients for C_{n_p} (subspace 1)[a]

Term	Coefficient	Standard errors	t for H_0 coefficient = 0	P value	Significance ($P < 0.05$)
Constant	0.24657	0.01109	22.239	0.000	Significant
M	0.03960	0.01090	3.632	0.008	Significant
α	0.32033	0.01090	29.386	0.000	Significant
M^2	−0.01108	0.01607	−0.689	0.513	Not significant
α^2	0.02654	0.01607	1.652	0.143	Not significant
$M\alpha$	0.04772	0.01335	3.574	0.009	Significant

[a]$R^2 = 99.22\%$, and $R^2(\text{adj}) = 98.67\%$.

Table 6 Estimated regression coefficients for C_{l_p} (subspace 1)[a]

Term	Coefficient	Standard errors	t for H_0 coefficient = 0	P value	Significance ($P < 0.05$)
Constant	−0.027369	0.000162	−169.338	0.000	Significant
M	0.001007	0.000159	6.335	0.000	Significant
α	−0.000343	0.000159	−2.161	0.068	Not significant
M^2	0.000175	0.000234	0.748	0.479	Not significant
α^2	0.000105	0.000234	0.449	0.667	Not significant
$M\alpha$	−0.000090	0.000195	−0.462	0.658	Not significant

[a]$R^2 = 86.84\%$, and $R^2(\text{adj}) = 77.45\%$.

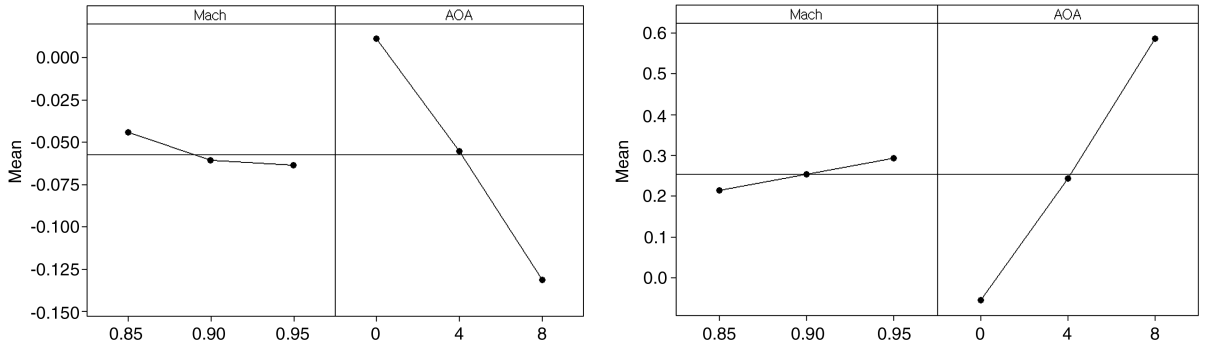

a) C_{Y_p} b) C_{n_p}

Fig. 5 Main effect plot for Magnus measurements (subspace 1).

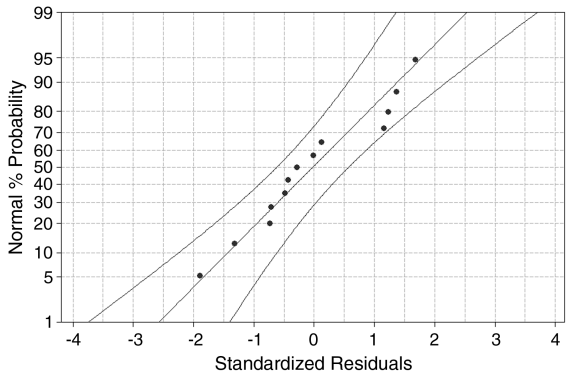

Fig. 6 Normal probability plot of residuals with a 95% confidence interval for C_{Y_p}.

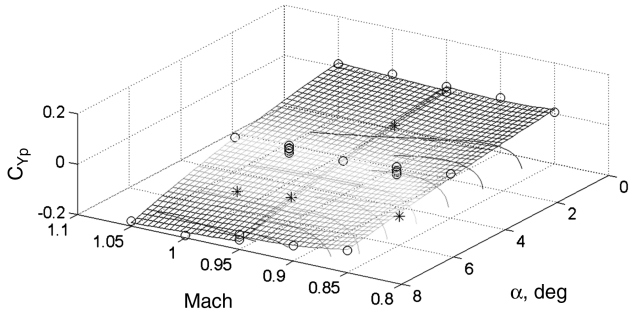

Fig. 7 Response surface for C_{Y_p}: subspace 1 and subspace 2.

The p value in the table for each regression coefficient tests the null hypothesis H_0 [19,20]. In general, a low p value suggests that the corresponding regressor variables x_i contribute significantly to the regression model. However, by comparing the t for H_0 values of M and α at a 5% level of significance, we see that α is a much more significant variable than M. We also find that the quadratic terms and interaction term, such as M^2, α^2, and $M\alpha$, are not important in this C_{Y_p} regression model. Table 5 also gives regression analysis results of C_{n_p} in coded units. The regression analysis results of C_{n_p} have similar characteristics of those of C_{Y_p}. We see that both M and α are significant variables in the C_{n_p} data, and the interaction term $M\alpha$ is more important than the other quadratic terms. The regression results given in Tables 4 and 5 indicate that the response surface is approximately linear in M and α. The various R^2 values (coefficient of determination) at the bottom of the table imply that the present regression model fits the data extremely well. The ANOVA tables (testing for a lack of fit) for C_{Y_p} and C_{n_p}, which are not presented here, also indicate that the regression models adequately describe the measured Magnus data.

The regression results for C_{l_p}, given in Table 6, indicate that the response surface shows less variation than the Magnus data and a slightly linear tendency in M. We see that α, M^2, α^2, and $M\alpha$ are not important for the C_{l_p} regression model. Because of the flat nature of the response surface, the present regression model fits the data less than the previous Magnus data.

The main effect plot by plotting of the means at each factor level of C_{Y_p} and C_{n_p} compared to the overall mean is shown in Fig. 5. By comparing the slopes of the lines of the main effect plot, the relative magnitude of the factor effects can be compared. The Mach number factor shows a smaller difference in the magnitude than the AOAs. Both Magnus parameters C_{Y_p} and C_{n_p} seem to be strongly affected by the AOA in the opposite direction of the slope.

To guarantee the validity of the regression model, we must always ensure that none of the regression assumptions [14,15] are violated. For this purpose, we checked the normality assumption by constructing normal probability plots of the residuals; the results are shown in Fig. 6. We see from Fig. 6 that the residuals are scattered around a straight line, which implies that the normality assumption is satisfied at a 5% level of significance. We also confirmed that the present regression curves do not violate the constant variance assumption and that the residuals are not correlated with each other. The normality plots of the residuals for C_{n_p} and C_{l_p} have characteristics similar to C_{Y_p}.

Figure 7 shows a response and contour plot of C_{Y_p} as functions of M and α for two subspaces. In this figure, the C_{Y_p} data from the measurement (13 data points for each subspace) are marked with circles. To check the adequacy of the response models, we also tested

Table 7 Validation test for C_{Y_p} (confirmation experiments)

	Mach	AOA	Measured	Prediction	95% PI low	95% PI high	Remark
Subspace 1	0.85	6	−0.08504	−0.07888	−0.110	−0.046	
	0.95	2	−0.03291	−0.02666	−0.059	+0.000	
	0.95	6	−0.10239	−0.10761	−0.140	−0.075	
Subspace 2	0.95	2	−0.03291	−0.02768	−0.060	+0.000	Subspace 1
	0.95	6	−0.10239	−0.11113	−0.140	−0.079	Subspace 1
	1.00	6	−0.12334	−0.11599	−0.140	−0.087	

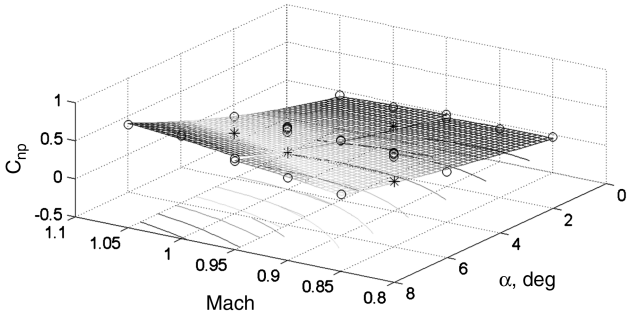

Fig. 8 Response surface for C_{n_p}: subspace 1 and subspace 2.

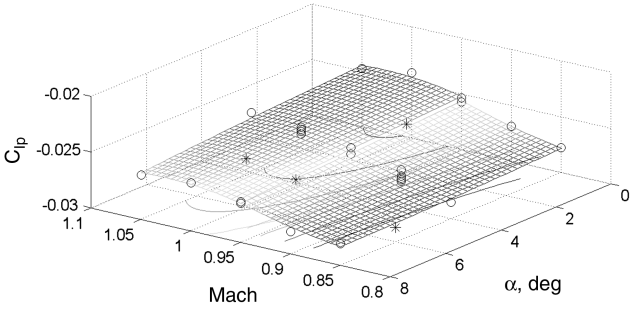

Fig. 9 Response surface for C_{l_p}: subspace 1 and subspace 2.

extra $M - \alpha$ combinations as confirmation experiments marked with asterisks. For example, the measured value for a confirmation point ($M = 0.85$ and $\alpha = 6$ deg) was compared with the prediction value from the regression model. Using our response models for subspace 1, we find that the 95% prediction intervals (PIs) for this confirmation point are $-0.110 \le C_{Y_p} \le -0.046$ and $0.28 \le C_{n_p} \le 0.42$. The actual measurement yielded values of $C_{Y_p} = -0.08504$ and $C_{n_p} = 0.35792$, which clearly demonstrate the accuracy of the present response model. Table 7 is the C_{Y_p} prediction results of the four confirmation experiments where the two data points ($M = 0.95$ and $\alpha = 2$ deg, and $M = 0.95$ and $\alpha = 6$ deg) were applied to both regression models at the same time. By comparing the measured values of C_{Y_p} at a 5% level of significance, we see that the regression models adequately describes the measured C_{Y_p} data.

Figure 8 shows the response plot of C_{n_p}. In this figure, the five circles overlapped at the center point of the FCCD test matrix for each subspace represent the repeatability of the response surface. We can easily see that the parameter C_{n_p} shows less variation than the C_{Y_p} at the subspace boundaries. Table 8 also shows the prediction results of the four confirmation experiments. Figure 9 shows the response plot of C_{l_p}. The validation test results of C_{l_p} characteristics are similar to the Magnus data.

B. Magnus Measurement Comparison

The validity of the Magnus measurement techniques was evaluated by comparing it with the Magnus test data obtained on the same configuration in the Arnold Engineering Development Center's Propulsion Tunnel 4T (AEDC-4T). Figure 10 shows Magnus measurement results [14] of the two wind tunnels (AEDC-4T and ADD-TSWT). The solid lines on the graph represent C_{Y_p} and C_{n_p}, which were obtained using a least-squares fit for each spin-decay measurement. These plots show the linear behavior of the side-force and yawing moment coefficients on spin parameter. This linearity implies that the Magnus force-and-moment derivatives are fairly constant within the range of the spin parameter tested. The dotted lines represent the 95% confidence intervals of the present measurements. We excluded outliers greater than $+3$ and less than -3 standard deviation of the residuals, which were considered potentially unusual.

Figure 11 presents the Magnus derivatives for various AOAs. These results were corrected by the zero offset values at $\alpha = 0$ deg, because there should be no Magnus effects at the zero AOA. The 95% confidence uncertainties (U_r) of the Magnus dynamic derivatives at

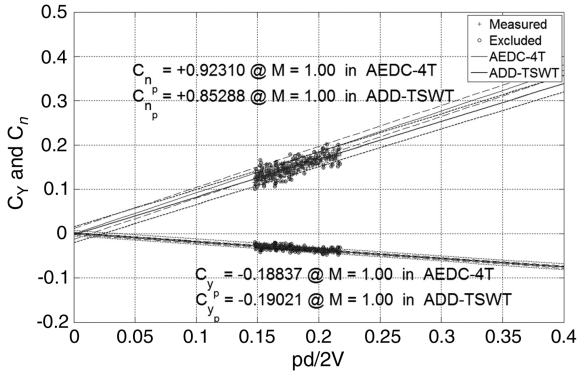

Fig. 10 Magnus measurement comparison at $\alpha = 8$ deg (subspace 2).

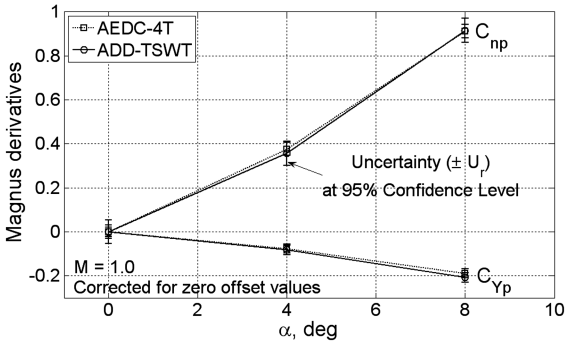

Fig. 11 Magnus measurement for various AOA (subspace 2).

$M = 1.0$ were found to lie between ± 0.0216 and ± 0.0546. Using the Magnus dynamic data and the uncertainties from this figure, we see that fair to good agreement is obtained with reasonable accuracy.

IV. Conclusions

High-speed wind-tunnel tests were conducted to efficiently characterize the dynamic Magnus effect and spin-damping derivatives for a spinning projectile model. To determine the relation between the Mach number and the AOA of a 155-mm spinning model, various tests based on the DOE theory were performed, and

Table 8 Validation test for C_{n_p} (confirmation experiments)

	Mach	AOA	Measured	Prediction	95% PI Low	95% PI High	Remark
Subspace 1	0.85	6	+0.35792	+0.35042	+0.280	+0.420	
	0.95	2	+0.14630	+0.10927	+0.036	+0.180	
	0.96	6	+0.45106	+0.47733	+0.400	+0.550	
Subspace 2	1.00	6	+0.56032	+0.53257	+0.450	+0.620	
	0.95	2	+0.14630	+0.09759	+0.000	+0.190	Subspace 1
	0.96	6	+0.45106	+0.47308	+0.380	+0.570	Subspace 1

the data was processed by using the RSM. The regression models were found to successfully estimate the Magnus effects and spin-damping coefficients required to investigate aerodynamic characteristics of a spinning projectile over the required experimental design space. With these statistical experimental design techniques, the number of tests required and the overall test hours in the wind-tunnel testing can be significantly reduced. Uncertainties can also be precisely determined with a specified level of confidence. The methodology used in this study is being considered to be expanded to determine other dynamic derivatives in wind-tunnel tests.

References

[1] Davis, B. S., Guidos, B. J., and Harkins, T. E., "Complementary Roles of Spark Range and Onboard Free-Flight Measurements for Projectile Development," U.S. Army Research Lab., ARL-TR-4910, Aug. 2009.

[2] DeSpirito, J., and Heavey K. R., "CFD Computation of Magnus Moment and Roll Damping Moment of a Spinning Projectile," AIAA Paper 2004-4713, Aug. 2004.

[3] Sahu, J., "Numerical Computations of Dynamic Derivatives of a Finned Projectile Using a Time-Accurate CFD Method," AIAA Paper 2007-6581, Aug. 2007.

[4] Sahu, J., "Transonic Navier–Stokes Computations for a Spinning Body of Revolution; Final Report," U.S. Army Ballistic Research Lab., BRL-TR-3265, Sept. 1991.

[5] Weinacht, P., "Projectile Performance, Stability, and Free-Flight Motion Prediction Using Computational Fluid Dynamics," *Journal of Spacecraft and Rockets*, Vol. 41, No. 2, March–April 2004, pp. 254–263.
doi:10.2514/1.1037

[6] Weinacht, P., "Characterization of Small-Caliber Ammunition Performance Using a Virtual Wind Tunnel Approach," AIAA Paper 2007-6579, Aug. 2007.

[7] DeSpirito, J., Silton, S. I., and Weinacht, P., "Navier-Stokes Predictions of Dynamic Stability Derivatives: Evaluation of Steady-State Methods," U.S. Army Research Lab., ARL-TR-4605, Sept. 2008.

[8] DeSpirito, J., "CFD Prediction of Magnus Effect in Subsonic to Supersonic Flight," U.S. Army Research Lab., ARL-TR-4929, Sept. 2009.

[9] Stahl, J., Costello, M., and Sahu, J., "Projectile Aerodynamics Coefficient Estimation Using Integrated CFD/RBD and Flight Control System Modeling," AIAA Paper 2009-5715, Aug. 2009.

[10] Stahl, J., "Computation of Unsteady Aerodynamics of a Spinning Body at Transonic Speeds," AIAA Paper 2009-3852, 22–25 June 2009.

[11] Marquart, E. J., "Re-Engineering of the Spin-Damping and Magnus Measurement Technique at AEDC," AIAA Paper 1998-0611, Jan. 1998.

[12] Prieur, J., and Sagnier, P., "New Testing Capabilities for the Supersonic Wind Tunnel S3MA of the ONERA MODANE Test Center," *95th Supersonic Tunnel Association International Meeting*, ONERA, 29 April–2 May 2001.

[13] Wincey, R. T., "Techniques for Determining Missile Parameters from a Wind Tunnel," Defense Intelligence Agency, MSC2 -TM-95-001, Oct. 1995.

[14] Ng, C. H., and Han, S., "155-mm Korean Extended Range Artillery Projectile Wind Tunnel Test Results," U. S. Army Armament Research, Development, and Engineering Center, Picatinny, NJ, Aug. 1996.

[15] Marquart, E. J., "Free-Spin Damping Measurement Techniques," AIAA Paper 1993-3457, 1993.

[16] Malcom, G. N., "Rotary and Magnus Balances," AGARD, LS-114, 1981, Chap. 6.

[17] Favaregh, N. M., and Landman, D., "Global Modeling of Pitch Damping from Flight Data," AIAA Paper 2006-6145, 2006.

[18] Omran, A., Landman, D., and Newman, B., "Stability Derivative Modeling Based on Aircraft Flight Modes Using Design of Experiments," AIAA Paper 2008-2532, 2008.

[19] Montgomery, D. C., *Design and Analysis of Experiments*, 6th ed., Wiley, Hoboken, NJ, 2005, pp. 373–463.

[20] Myers, R. H., and Montgomery, D. C., *Response Surface Methodology: Process and Product Optimization Using Designed Experiments*, 1st ed., Wiley, New York, 1995, pp. 1–123, 208–265.

[21] DeLoach, R., "Application of Modern Experiment Design to Wind Tunnel Testing at NASA Langley Research Center," 36th Aerospace Sciences Meeting and Exhibit, AIAA Paper 1998-0713, Jan. 12–15, 1998.

[22] DeLoach, R., "Tailoring Wind Tunnel Data Volume Requirements Through The Formal Design Of Experiments," 20th Advanced Measurement Technology and Ground Testing Conference, AIAA Paper 1998-2884,June 1998.

[23] DeLoach, R., "Improved Quality in Aerospace Testing Through the Modern Design of Experiments," 38th Aerospace Sciences Meeting and Exhibit, AIAA Paper 2000-0825, Jan. 2000.

[24] DeLoach, R., and Cler, D. L., "Fractional Factorial Experiment Design to Minimize Configuration Changes in Wind Tunnel Testing," *40th Aerospace Sciences Meeting and Exhibit*, AIAA Paper 2002-0746, Jan. 2002.

[25] DeLoach, R., "MDOE Perspectives on Wind Tunnel Testing Objectives," Advanced Measurement Technology and Ground Testing Conference, AIAA Paper 2002-2796, June 2002.

[26] Landman, D., Simpson, J., Hall, B., and Sumner, T., "Use of Designed Experiments in Wind Tunnel Testing of Performance Automobiles," Proceeding of the 2002 SAE Motorsports Engineering Conference and Exhibition (P-382), SAE International Paper 2002-01-3313, Warrendale, PA, Dec. 2002.

[27] DeLoach, R., "The Modern Design of Experiments for Configuration Aerodynamics: A Case Study," Aerospace Sciences Meeting and Exhibit, 44th, AIAA Paper 2006-0923, Jan. 2006.

[28] Landman, D., Simpson, J., Mariani, R., Oritz, F., and Britcher, C., "Hybrid Design for Aircraft Wind-Tunnel Testing Using Response Surface Methodologies," *Journal of Aircraft*, Vol. 44, No. 4, July–Aug. 2007, pp. 1214–1221.
doi:10.2514/1.25914

[29] Landman, D., Simpson, J., Vicroy, D., and Parker, P., "Response Surface Methods for Efficient Complex Aircraft Configuration Aerodynamic Characterization," *Journal of Aircraft*, Vol. 44, No. 4, July–Aug. 2007, pp. 1189–1195.
doi:10.2514/1.24810

[30] Oh, Se-Yoon, and Park, Seung, O., "Optimal Aft End Distorted Fin Model Using Response Surface Method," *Journal of Spacecraft and Rockets*, Vol. 46, No. 3, May–June 2009, pp. 592–598.
doi:10.2514/1.40496

[31] "Assessment of Experimental Uncertainty with Application to Wind Tunnel Testing," AIAA Standard S-017A-1999, 1999.

[32] Coleman, H. W., and Steele, W. G. Jr., *Experimentation and Uncertainty Analysis for Engineers*, Wiley, New York, 1999, pp. 16–43.

[33] Minitab, Statistical Software Package, Ver. 15.1.0.0, Minitab, State College, PA, 2006.

[34] Design-Expert, Statistical Software Package, Ver. 7.0.0, Stat-Ease, Minneapolis, 2005.

M. Miller
Associate Editor